SCIENCE CHINA Materials

ARTICLES

mater.scichina.com link.springer.com

Published online 23 August 2016 | doi: 10.1007/s40843-016-5072-5
Sci China Mater 2016, 59(8): 609–617

A surfactant-free route to synthesize $Ba_xSr_{1-x}TiO_3$ nanoparticles at room temperature, their dielectric and microwave absorption properties

Qing-Song Wu, Jian-Wei Liu*, Guang-Sheng Wang, Shao-Feng Chen and Shu-Hong Yu*

ABSTRACT Perovskite materials, such as $Ba_xSr_{1-x}TiO_3$ (BST), have been continuously receiving attentions due to their unique ferroelectric, pyroelectric, dielectric, piezoelectric and electric-optic properties. Here, we report a facile route for the synthesis of BST nanocrystalline materials by fast mixing of MCl_2 (M = Ba, Sr) aqueous solution and titanium isopropoxide ethanol solution at room temperature without using any surfactants or structure-directing templates. The molar ratio of Ba/Sr was controlled by adjusting the original molar ratio of $BaCl_2{\cdot}2H_2O$ and $SrCl_2{\cdot}6H_2O$. The dielectric properties and microwave absorption capability of the BST nanocrystalline were studied. The results indicate that the BST nanocrystalline material has the best dielectric and microwave absorption properties in the case of $Ba_{0.7}Sr_{0.3}TiO_3$. The present strategy is facile, low cost and high yield, which may provide a new route for the synthesis of other perovskite materials.

Keywords: perovskite, crystallization, dielectric, microwave absorption, mixed solution

INTRODUCTION

Perovskite materials, such as $Ba_xSr_{1-x}TiO_3$ (BST), have been continuously receiving attentions and widely studied in the past several decades because of their excellent ferroelectric, pyroelectric, dielectric, piezoelectric and electric-optic properties, which depend on the component, size and crystalline structure [1–2]. Barium titanate ($BaTiO_3$) which has a high dielectric constant is used in capacitor, piezoelectric sensor, and electronic-optical transducer [3–6]. The transition temperature of $BaTiO_3$ (T_c) from paraelectric phase to ferroelectric phase is 130°C. The replacement of Sr atom to Ba atom could reduce the T_c and change the phase, which affects the electric properties. For example, $Ba_{0.7}Sr_{0.3}TiO_3$ has the highest dielectric constant in BST materials at room temperature, which has the potential application in dynamic random-access memory (DRAM), tuneable filter, and oscillator, etc. [7,8].

The traditional synthetic route of perovskite materials is through sintering at above 1000°C. Several chemical methods have been developed for the low-temperature preparation of micro- and nano-sized perovskite crystals such as molten salt synthesis [9–10], solvothermal and hydrothermal method [11–17], decomposition of bimetallic alkoxide precursors [18–20], microwave route [21–24], and biosynthesis [25]. Though these routes offer successful synthesis of perovskite nanoparticles with high quality and good crystalline, they usually require temperatures higher than 100°C or expensive reactants. The thermodynamic modelling work by Riman and co-workers [26–29] indicated that alkaline-earth titanates could be synthesized in aqueous solution even at temperatures below 100°C when the pH value was appropriate. It is highly expected to find a synthetic route to obtain BST materials at room temperature, ambient pressure, and high productivity with reactants very accessible [30].

On the other hand, electromagnetic interference (EMI) shielding problems in the fields of electromagnetic wave communications have attracted intense attentions and various types of microwave absorbers have been developed. Many researchers have focused on the development of high-efficient electromagnetic wave absorbers with strong absorption characteristics, wide absorption frequency, lightweight and antioxidation. The dielectric relaxation effect of $BaTiO_3$ in the gigahertz frequency bands can lead

Division of Nanomaterials & Chemistry, Hefei National Laboratory for Physical Science at Microscale, Collaborative Innovation Center of Suzhou Nano Science and Technology, Department of Chemistry, University of Science and Technology of China, Hefei 230026, China
* Corresponding authors (emails: shyu@ustc.edu.cn (Yu SH); jwliu13@ustc.edu.cn (Liu JW))

to dielectric loss. The microwave absorption using $BaTiO_3$ (BT) ceramic in bulk size as ferroelectric component has been investigated previously. To date, previous studies about the dependency of electromagnetic properties on the morphology of microwave absorbers indicate that geometrical shape of the microwave absorbers plays a key role in the microwave absorption properties. However, the addition of Sr atoms to replace partial Ba in the BT, which affects the absorption properties of the BT, has not been studied.

Herein, we report a simple and versatile strategy to synthesize the BST nanoparticles under ambient conditions in an ethanol/water mixed solution based on our previous work [31]. In this approach, a series of BST nanocrystalline particles with good crystalline, pure phase, uniform size, and high yield can be prepared at room temperature by simply mixing $BaCl_2{\cdot}2H_2O$, $SrCl_2{\cdot}6H_2O$ and titanium isopropoxide in water/ethanol solution for about 6 h. The dielectric properties and microwave absorption capability of the BST were studied, showing that the BST nanocrystalline material shows the best dielectric and microwave absorption properties when $x = 0.7$.

EXPERIMENTAL SECTION

Materials

All chemicals are analytical grade and used as received without further purification. In a typical procedure, $BaCl_2{\cdot}2H_2O$ and $SrCl_2{\cdot}6H_2O$ (1.5 mmol in all) and a certain amount of KOH were dissolved in 5 mL of deionized water respectively and mixed together to form a homogeneous solution. 1.5 mmol of titanium isopropoxide were added into 10 mL of ethanol. The mole ratio of (Ba+Sr)/Ti was 1. Then, the two solutions were mixed quickly within 20 s under vigorous stirring with immediate formation of a white gelatinous suspension precursor, which was aged at room temperature for about 6 h. The white precipitates (~2.6 g, the yield > 90%) were washed away by distilled water and absolute ethanol, respectively, and dried in a vacuum at 30°C for 4 h. A series of $Ba_xSr_{1-x}TiO_3$ nanocrystalline with different x value (from 0 to 1) could be obtained by adjusting the original molar ratio of $BaCl_2{\cdot}2H_2O$ and $SrCl_2{\cdot}6H_2O$.

Characterization

X-ray powder diffraction (XRD) was carried out on the substrate by Philips X'Pert Pro Super Diffratometer CuKα radiation (λ = 1.541874 Å). Scanning electron microscopy (SEM) images were obtained by JEOL JSM-6700F and Karl Zeiss Supra 40. Transmission electron microscopy (TEM), high-resolution TEM (HRTEM) images and electron diffraction (ED) patterns were obtained on a JEOL JSM-2010 microscope at an accelerating voltage of 200 kV. Energy-dispersive X-ray (EDX) analysis was obtained with an EDAX detector installed on the same HRTEM. To measure the dielectric property, the BST powders were grinded and tableted by using 5% polyvinyl acetate (PVA) as cross-linking agent and sintered to 1200°C under air atmosphere. The sinter temperature was maintainied at 500°C for several hours to remove the PVA. The dielectric constant was measured by Agilent 4294A precise impedance analyzer. In order to examine the microwave absorption of the BST, specimens were prepared by dispersing the BST powders into paraffin with a weight ratio of 1:1. After pressing the mixture into the cylindrical mould, the specimens with the thickness of 3 mm, the external diameter of 7 mm, and the inner diameter of 3 mm can be prepared. The microwave absorption capability was measured on Agilent PNA-L network Analyzer N5230C.

RESULTS AND DISCUSSION

The element concentrations of Ba and Sr in the final products were measured by inductively coupled plasma-atomic emission spectrometry (ICP-AES). The x value of $Ba_xSr_{1-x}TiO_3$ was calculated as listed in Table 1. Compared with the x value calculated from the initial weight ratio of reagents, the linear fit keeps as the same (Fig. 1).

Fig. 2 shows the XRD patterns of $BaTiO_3$ and $SrTiO_3$ products. All diffraction peaks of these samples can match the standard pattern of cubic $BaTiO_3$ (JCPDS No. 31-0174) and cubic $SrTiO_3$ (JCPDS No. 86-0179) quite well. No diffraction peaks of $BaCO_3$ and $SrCO_3$ or other impurities were detected, indicating that the obtained products are

Table 1 The element concentration of Sr and Ba measured by ICP-AES, and the x value of $Ba_xSr_{1-x}TiO_3$ calculated from element concentration

Sample	Element concentration (mass%)		Value of x
	Sr	Ba	
BS1	34.46	6.11	0.10163
BS2	29.35	11.38	0.19832
BS3	25.66	16.54	0.29141
BS4	21.36	21.65	0.39272
BS5	17.62	26.39	0.48865
BS6	13.22	30.01	0.59156
BS7	10.39	37.08	0.69484
BS8	6.27	39.30	0.79996
BS9	3.29	44.43	0.89601

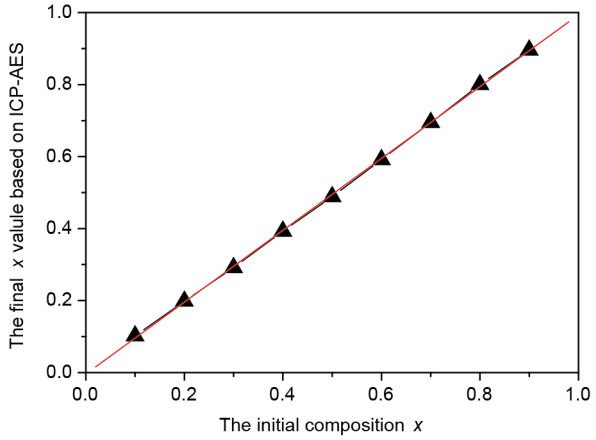

Figure 1 Linear fit of the original mole concentration of Ba and the x value of the final BST samples. $Y = a + bx$, $a = -0.004$, $b = 0.99802$.

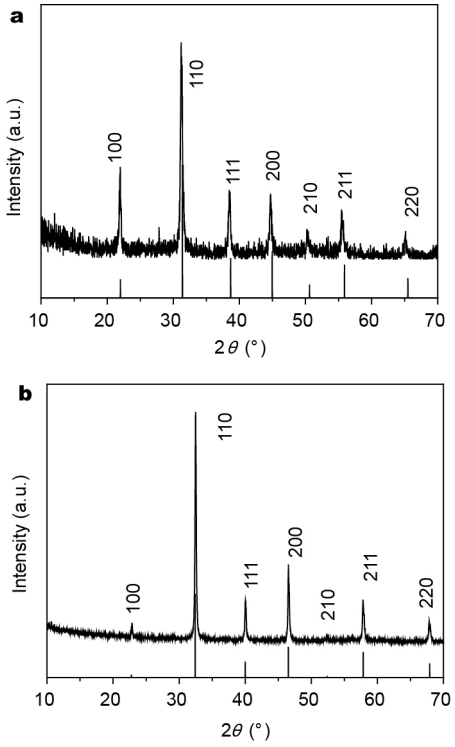

Figure 2 XRD patterns of the final products: (a) $BaTiO_3$ and (b) $SrTiO_3$.

pure $BaTiO_3$ and $SrTiO_3$ without the formation of carbonate. This result reveals that the samples prepared at room temperature are all pure cubic phase, even without N_2 atmosphere protection.

A series of $Ba_xSr_{1-x}TiO_3$ samples with the x value varied from 0 to 1 (step = 0.1) can be prepared by controlling the original molar ratio of Ba^{2+} and Sr^{2+} in the reagents. The XRD patterns of the serials samples shown in Fig. 3 indicate that each diffraction peak is a single and intact without splitting, which means the Ba ion is incorporated into the $SrTiO_3$ lattice to replace the Sr ion, without any phase separation or superlattice phenomenon. If the final product was a superlattice structure, the peak separation could be found in the XRD pattern, which was previously reported by Lee *et al.* [32].

From Fig. 3, we could also found that the 2θ value of each peak changed with different x value. When the x value increased from 0 to 1, the 2θ value of each peak was reduced. That was because the radius of Ba atom was bigger than Sr atom. With the replacement of Ba ion by Sr ion, the lattice constant was changed and the d value of the interplanar spacing would increase. As a result, the 2θ value reduced. Taking the (200) plane for example (Fig. 4a), the 2θ value reduced from 46.1° to 44.7°, when the x value increased from 0 to 1. Converting the d value, the interplanar spacing increased from 3.92 Å to 4.04 Å (Fig. 4b). Su *et al.* [33] reported that when the x value was in the region of 0.4 to 0.6, the crystalline of product was not good, and the (111) peak would change a lot because the trigonal geometry of Ba/Sr in (111) plane was more sensitive to the change of component than the tetragonal geometry in (200) plane. However, this phenomenon was not observed in our experiment and the crystallinity of our BST samples was good. We could find the change of the relative intensity between (111) plane and (200) plane. When $x = 0$, the relative intensity of (111) plane was weaker than that of (200) plane. By increasing the x value, the relative intensity of (111) plane enhanced. It depends on the exposure of the different plane. From SEM images of the BST samples in Fig. 5, it was found that when the x value increased from 0 to 1, the morphology of samples changed from cubic to sphere. The exposure of (200) plane was higher than (111)

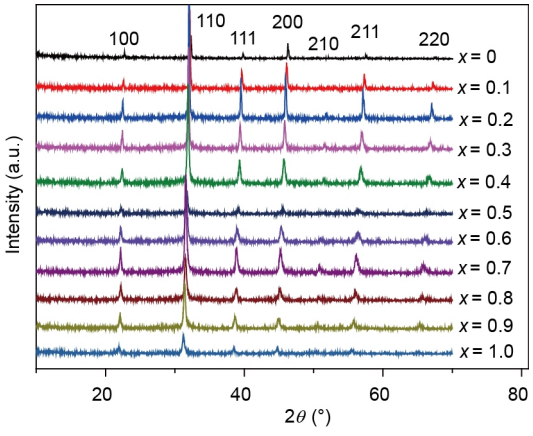

Figure 3 XRD patterns of the BST products. The x value was varied from 0 to 1.

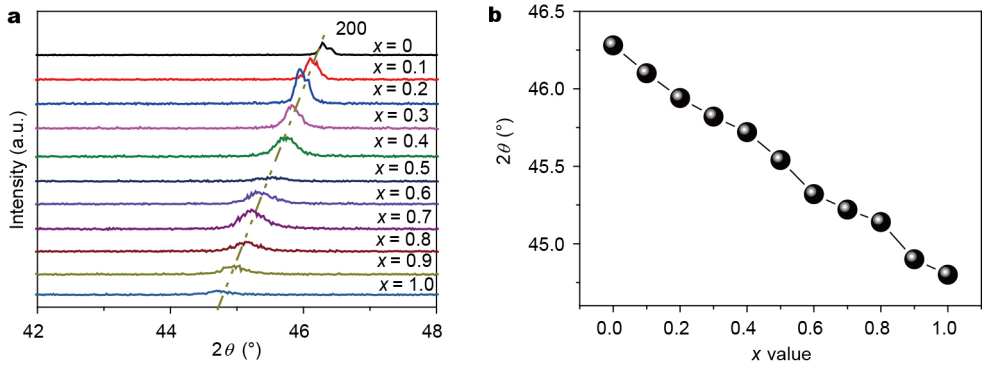

Figure 4 (a) The (200) peak in XRD patterns of BST samples, and (b) the relationship of 2θ and x value.

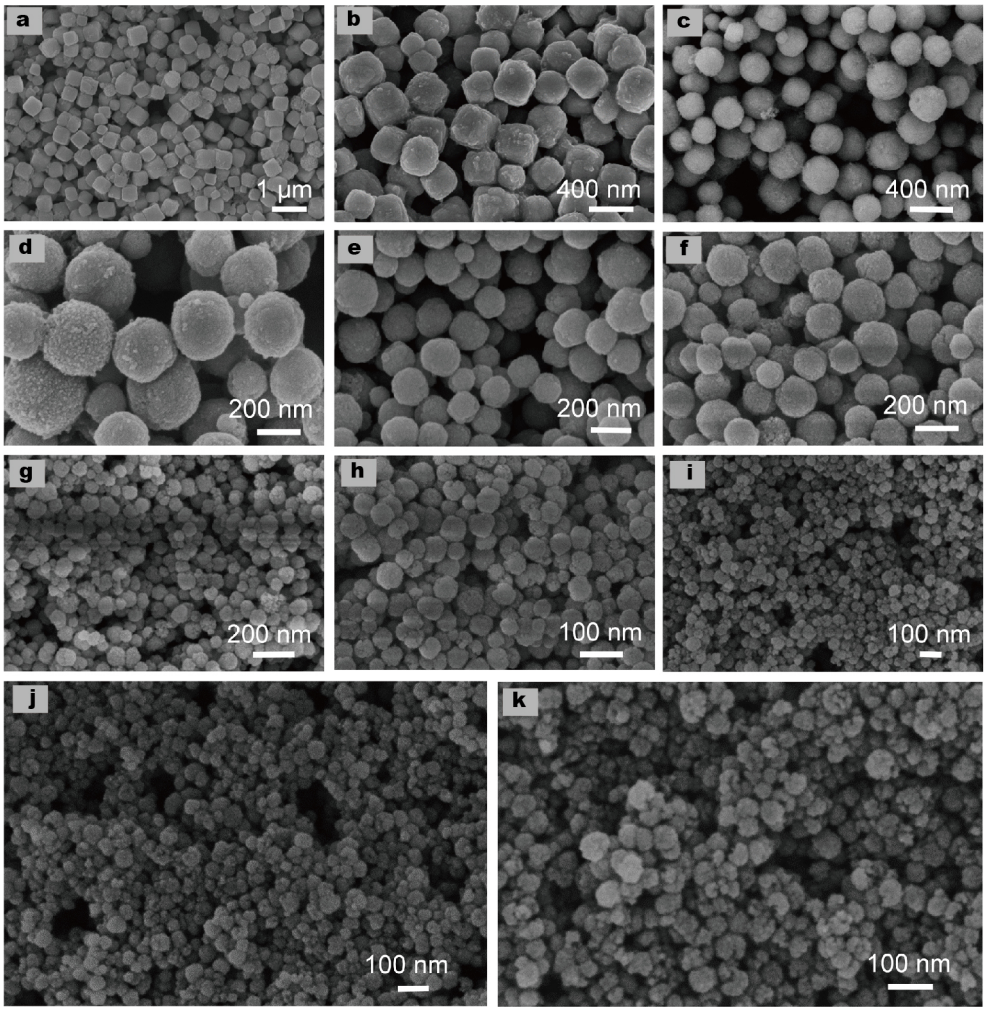

Figure 5 SEM images of the BST samples: (a)–(k) the samples with x value from 0 to 1 (step 0.1).

plane in cubic, so the relative intensity of (200) plane was stronger than that of (111) plane. When the morphology of the sample was sphere-like structure, there was little difference of the relative intensity, because the exposure of (200) plane and (111) plane was nearly the same.

As shown in Fig. 5, the size of particles decreases with the increase of the x value. By increasing the concentration of Ba ions, the particle size decreases from ~500 nm to

~50 nm. The only exception is $Ba_{0.7}Sr_{0.3}TiO_3$ whose particle size is bigger than that of $Ba_{0.6}Sr_{0.4}TiO_3$. The calculation of molecular dynamics shows that when $x = 0.7$, there is a balance between the opposing effects of extra space and lattice shrinkage to allow the displacement of Ti^{4+} to reach the maximum [34]. Some unique physical properties appear in the $Ba_{0.7}Sr_{0.3}TiO_3$, such as ultra-high dielectric constant, which fit the calculation result and reports in bulk crystals [35–37]. The same phenomenon of the change of morphology and particle size was also observed in TEM images (Fig. S1), which was different from the previous report. Lee *et al*. [32] found that the particle size of $BaTiO_3$ was bigger than that of $SrTiO_3$ and the size of $Ba_{0.7}Sr_{0.3}TiO_3$ was smaller than $BaTiO_3$ and $SrTiO_3$, with the synthesis temperature at 80°C. Demirörs *et al*. [38] found that $BaTiO_3$, $SrTiO_3$ and $Ba_{0.5}Sr_{0.5}TiO_3$ had the same size distribution. In this system, the crystallization process of $SrTiO_3$ and $BaTiO_3$ nanocrystals obeys the Ostwald ripening process. It was found that the final $SrTiO_3$ particles were single crystalline cubes, and the $BaTiO_3$ particles were polycrystalline spherical aggregates of nanoparticles (Figs 2 and 5). Time-dependent experiments were carried out to understand the crystallization process. As shown in Fig. S2, small amorphous nanoparticles formed at initial stage and they were further agglomerated, dissolved or recrystallized. For $SrTiO_3$, after aging for 2 h, amorphous particles directly grew into cubes with size of ~300 nm (Figs S2a and b), which would grow bigger with increasing the aging time. For $BaTiO_3$, after aging for 2 h, amorphous particles grew into particles with size of around 10 nm (Figs S2c and d), which would aggregate into spherical particles (50 nm) with increasing the aging time. Therefore, initial nucleation (2 h) of $SrTiO_3$ and $BaTiO_3$ is different, leading to different final forms of crystals (single-crystalline $SrTiO_3$ and polycrystalline $BaTiO_3$) during the Ostwald ripening process. Furthermore, Tanaka *et al*. [34] pointed out that by increasing the concentration of Ba ions in $Ba_xSr_{1-x}TiO_3$, the particle size decreased, which were compatible with our results.

BST has been widely used because of its high dielectric constant at room temperature. In this experiment, the BST powders were grinded and tableted by using 5% PVA as cross-linking agent and sintered to 1200°C under air atmosphere. The sinter temperature was maintained at 500°C for several hours to remove PVA. The dielectric constant was measured by Agilent 4294A precise impedance analyzer. The following formula was used to calculate the dielectric constant ε_r:

$$\varepsilon_r = (C \times d) / (\varepsilon_0 \times A), \quad (1)$$

where ε_r is the dielectric constant, C the capacitance, d the thickness of tablet, A the area of tablet, ε_0 the dielectric distant of air. Fig. 6 shows the relationship between the dielectric constant and frequency. It was found that when x value increased from 0 to 0.4, the dielectric property was not as good as that of the commercial BST powder (CBST, $x = 0.8$). When $x \geq 0.5$, the BST sample shows better dielectric property than CBST obviously. It is notable that when $x \geq 0.7$, the dielectric constant increases from ~400 to ~3000. Even if the $Ba_{0.9}Sr_{0.1}TiO_3$ and $BaTiO_3$ has a better dielectric property in medium frequency (<10,000 Hz), their dielectric constant decreases very quickly in high frequency (>10,000 Hz). The $Ba_{0.7}Sr_{0.3}TiO_3$ has much higher dielectric constant than all other BST samples. Firstly, it was found that the particle size was one of the important factors to affect the dielectric and microwave absorption properties of the $Ba_xSr_{1-x}TiO_3$ which was reported previously [39,40]. Secondly, besides the influence of the particle size, the polarization was also a key factor contributing to the microwave absorptions. With the increase of the concentration of Sr atom, the maximum of polarization moved from high temperature to low temperature in the same frequency. At the same time, $Ba_{0.7}Sr_{0.3}TiO_3$ reached the maximum of polarization exactly at room temperature. Hence, $Ba_{0.7}Sr_{0.3}TiO_3$ shows higher performance in dielectric constant than other BST powders at room temperature which was reported by Pramanik *et al*. [41]. At room temperature, $Ba_{0.7}Sr_{0.3}TiO_3$ reached the maximum of polarization exactly. The performance in dielectric constant of $Ba_{0.7}Sr_{0.3}TiO_3$ was higher than other BST powders at room temperature, which could make it have promising applications in many technical fields.

As a unique dielectric material, BST has potential application in microwave absorption at gigahertz frequencies [42,43]. There are three factors contributing to the microwave absorption mechanisms, i.e., the dominant dielectric polarization, spontaneous polarization, and the associated relaxation effects [39]. It is well known that changing the coating thickness of the absorber is an available way to tune the microwave absorption frequency according to the transmission line theory. Also the structure and the morphology of the materials may play a key role on their microwave absorption performance [40,44]. The nawow size distribution and uniform morphology of our BST samples are interesting for investigation of their microwave absorption property. The reflection loss (RL) of the BST/paraffin composites was calculated using the transmission line theory [45,46]:

$$Z_{in} = (\mu / \varepsilon)^{1/2} \tanh[-j(2\pi f d / c)(\mu\varepsilon)^{1/2}], \quad (2)$$

$$\mathrm{RL}(dB) = -20\log_{10} | (Z_{in} - 1) / (Z_{in} + 1) |, \quad (3)$$

where ε is the relative complex permittivity, μ the permeability of the absorber, Z the input impedance of the absorber, f the frequency of microwave, d the thickness of the absorber and c the velocity of light.

Fig. 7a shows the RL of the $Ba_{0.7}Sr_{0.3}TiO_3$-parraffin composite of different thickness, indicating a maximum RL of −11.25 dB at 12 GHz with the film thickness of 3.0 mm. Fig. 7b shows the frequency dependency of the complex permittivity real part ε', permittivity imaginary part ε'', permeability real part μ', and permeability imaginary part μ'' of the $Ba_{0.7}Sr_{0.3}TiO_3$-parraffin composite. The real part μ' and imaginary part μ'' nearly remain constant with frequency, indicating that $Ba_{0.7}Sr_{0.3}TiO_3$ could hardly produce any magnetic loss. The lower real part value ε' is an advantage to keep a balance between permeability and permittivity, decreasing the reflection coefficient of the absorber [42]. Here we observed that the value of ε' declined from 5.8 to 4.5 with the frequency increasing from 11.52 to 12.4 GHz, which just corresponded to the effective RL region. Meanwhile, the ε'' value shows a remarkable peak in the same frequency region. From 2 to 10.56 GHz, the ε'' value keeps nearly constant, and changes upward with the frequency increasing from 10.56 to 11.92 GHz, then tends downward in the region of 11.92 to 13 GHz, which is due to the electric dipole moment rearrangement under the varying electromagnetic field, thus giving the high RL in this frequency region. Compared to other BST samples, we found that the $Ba_{0.7}Sr_{0.3}TiO_3$ still shows a much stronger RL (Figs S3–S12). The SEM images about the fracture surface of the measured BST samples were shown in Fig. S13. Analyzed from the microwave absorption data of $Ba_xSr_{1-x}TiO_3$ nanoparticles, it is reasonable to conclude that the concentration of Sr can remarkably affect the microwave absorption properties of $Ba_xSr_{1-x}TiO_3$ nanoparticles. There are two dominant factors contributing to the microwave absorption mechanism, i.e., the inherent electronic polarization resulted from $BaTiO_3$ and $SrTiO_3$ [42,47] and the interfacial polarization between the $BaTiO_3$ and $SrTiO_3$ [48].

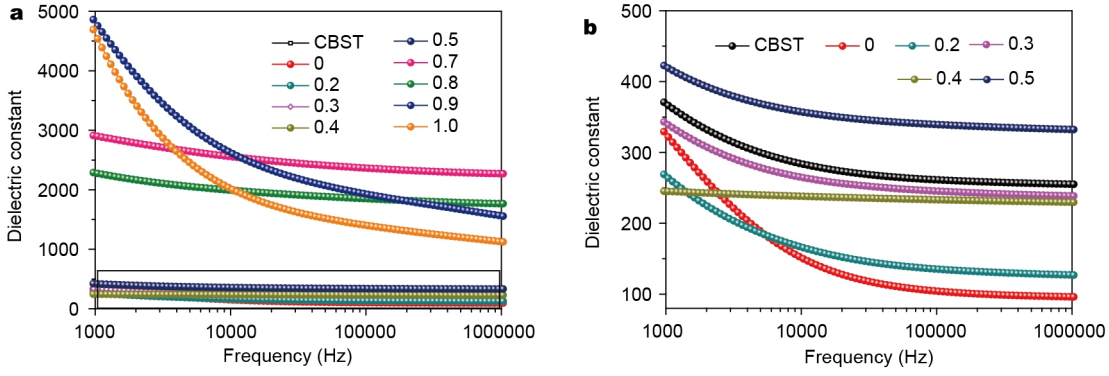

Figure 6 The relationship between dielectric constant and frequency. (a) The serials BST samples, (b) magnified view when x value was varied from 0 to 0.5.

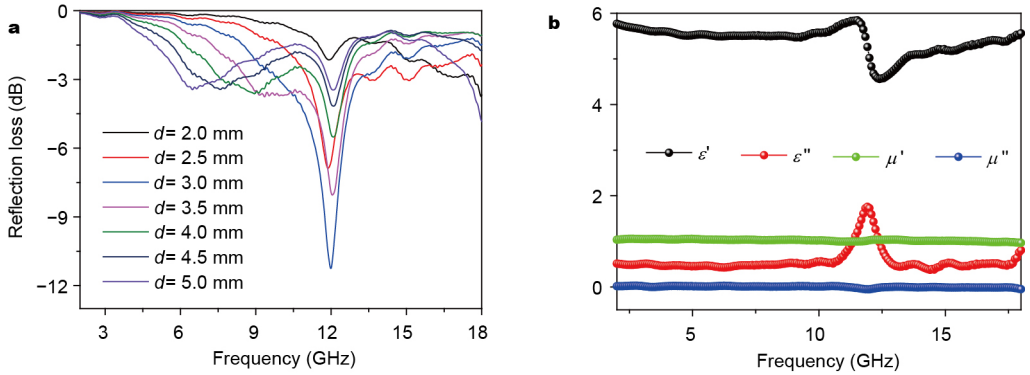

Figure 7 (a) RL of the $Ba_{0.7}Sr_{0.3}TiO_3$-paraffin composite of different thicknesses. (b) Complex permittivity and permeability of the $Ba_{0.7}Sr_{0.3}TiO_3$-paraffin composite.

CONCLUSION

In summary, we developed a simple and versatile route to synthesize the BST nanoparticles under ambient conditions in an ethanol/water mixed solution. A series of BST nanoparticles with good crystallinity, pure phase, uniform size, and high yield can be synthesized. The dielectric properties and microwave absorption capability of the BST with different composition were investigated. The results demonstrate that the BST materials have the best dielectric and microwave absorption properties when the composition $x = 0.7$. This surfactant-free route may be extended to synthesize other perovskite materials with tuneable compositions at room temperature.

Received 24 May 2016; accepted 9 June 2016; published online 23 August 2016

1 Chandler CD, Roger C, Hampden-Smith MJ. Chemical aspects of solution routes to perovskite-phase mixed-metal oxides from metal-organic precursors. Chem Rev, 1993, 93: 1205–1241
2 Peña MA, Fierro JLG. Chemical structures and performance of perovskite oxides. Chem Rev, 2001, 101: 1981–2018
3 Xing X, Deng J, Chen J, *et al.* Phase evolution of barium titanate from alkoxide gel-derived precursor. J Alloys Compounds, 2004, 384: 312–317
4 Dutta PK, Asiaie R, Akbar SA, *et al.* Hydrothermal synthesis and dielectric properties of tetragonal $BaTiO_3$. Chem Mater, 1994, 6: 1542–1548
5 Hennings D, Klee M, Waser R. Advanced dielectrics: bulk ceramics and thin films. Adv Mater, 1991, 3: 334–340
6 Choi KJ. Enhancement of ferroelectricity in strained $BaTiO_3$ thin films. Science, 2004, 306: 1005–1009
7 Selmi F, Komarneni S, Varadan VK, *et al.* Microwave sintering of Sb-doped SnO_3. Mater Lett, 1990, 10: 235–238
8 Fu C, Cai W, Chen H, *et al.* Voltage tunable $Ba_{0.6}Sr_{0.4}TiO_3$ thin films and coplanar phase shifters. Thin Solid Films, 2008, 516: 5258–5261
9 Liu H, Hu C, Wang ZL. Composite-hydroxide-mediated approach for the synthesis of nanostructures of complex functional-oxides. Nano Lett, 2006, 6: 1535–1540
10 Mao Y, Banerjee S, Wong SS. Large-scale synthesis of single-crystalline perovskite nanostructures. J Am Chem Soc, 2003, 125: 15718–15719
11 Dong W, Li B, Li Y, *et al.* General approach to well-defined perovskite $MTiO_3$ (M = Ba, Sr, Ca, and Mg) nanostructures. J Phys Chem C, 2011, 115: 3918–3925
12 Wang X, Zhuang J, Peng Q, *et al.* A general strategy for nanocrystal synthesis. Nature, 2005, 437: 121–124
13 Joshi UA, Lee JS. Template-free hydrothermal synthesis of single-crystalline barium titanate and strontium titanate nanowires. Small, 2005, 1: 1172–1176
14 Niederberger M, Garnweitner G, Pinna N, *et al.* Nonaqueous and halide-free route to crystalline $BaTiO_3$, $SrTiO_3$, and $(Ba,Sr)TiO_3$ nanoparticles via a mechanism involving C–C bond formation. J Am Chem Soc, 2004, 126: 9120–9126
15 Dong L, Shi H, Cheng K, *et al.* Shape-controlled growth of $SrTiO_3$ polyhedral submicro/nanocrystals. Nano Res, 2014, 7: 1311–1318
16 Kalyani V, Vasile BS, Ianculescu A, *et al.* Hydrothermal synthesis of $SrTiO_3$ mesocrystals: single crystal to mesocrystal transformation induced by topochemical reactions. Cryst Growth Des, 2012, 12: 4450–4456
17 Leoni M, Viviani M, Nanni P, *et al.* Low-temperature aqueous synthesis (LTAS) of ceramic powders with perovskite structure. J Mater Sci Lett, 1996, 15: 1302–1304
18 Urban JJ, Yun WS, Gu Q, *et al.* Synthesis of single-crystalline perovskite nanorods composed of barium titanate and strontium titanate. J Am Chem Soc, 2002, 124: 1186–1187
19 Brutchey RL, Morse DE. Template-free, low-temperature synthesis of crystalline barium titanate nanoparticles under bio-inspired conditions. Angew Chem Int Ed, 2006, 45: 6564–6566
20 Nuraje N, Su K, Haboosheh A, *et al.* Room temperature synthesis of ferroelectric barium titanate nanoparticles using peptide nanorings as templates. Adv Mater, 2006, 18: 807–811
21 Nyutu EK, Chen CH, Dutta PK, *et al.* Effect of microwave frequency on hydrothermal synthesis of nanocrystalline tetragonal barium titanate. J Phys Chem C, 2008, 112: 9659–9667
22 Moreira ML, Mambrini GP, Volanti DP, *et al.* Hydrothermal microwave: a new route to obtain photoluminescent crystalline $BaTiO_3$ nanoparticles. Chem Mater, 2008, 20: 5381–5387
23 Ma Y, Vileno E, Suib SL, *et al.* Synthesis of tetragonal $BaTiO_3$ by microwave heating and conventional heating. Chem Mater, 1997, 9: 3023–3031
24 Souza AE, Santos GTA, Barra BC, *et al.* Photoluminescence of $SrTiO_3$: influence of particle size and morphology. Cryst Growth Des, 2012, 12: 5671–5679
25 Bansal V, Poddar P, Ahmad A, *et al.* Room-temperature biosynthesis of ferroelectric barium titanate nanoparticles. J Am Chem Soc, 2006, 128: 11958–11963
26 Lencka MM, Riman RE. Thermodynamic modeling of hydrothermal synthesis of ceramic powders. Chem Mater, 1993, 5: 61–70
27 Lencka MM, Riman RE. Synthesis of lead titanate: thermodynamic modeling and experimental verification. J Am Ceramic Soc, 1993, 76: 2649–2659
28 Lencka MM, Riman RE. Thermodynamics of the hydrothermal synthesis of calcium titanate with reference to other alkaline-earth titanates. Chem Mater, 1995, 7: 18–25
29 Lencka MM, Nielsen E, Anderko A, *et al.* Hydrothermal synthesis of carbonate-free strontium zirconate: thermodynamic modeling and experimental verification. Chem Mater, 1997, 9: 1116–1125
30 Beier CW, Cuevas MA, Brutchey RL. Room-temperature synthetic pathways to barium titanate nanocrystals. Small, 2008, 4: 2102–2106
31 Wu QS, Liu JW, Chen SF, *et al.* Surfactant-free synthesis of $SrTiO_3$ hierarchical structures in ethanol/water mixed solvent at room temperature. CrystEngComm, 2015, 17: 6895–6900
32 Lee J, Kim L, Kim J, *et al.* Dielectric properties of $BaTiO_3/SrTiO_3$ oxide superlattice. In: Fundamental Physics of Ferroelectrics. American Institute of Physics Conference Proceeding Washington DC, 2002, 626: 178–187
33 Su K, Nuraje N, Yang NL. Open-bench method for the preparation of $BaTiO_3$, $SrTiO_3$, and $Ba_xSr_{1-x}TiO_3$ nanocrystals at 80°C. Langmuir, 2007, 23: 11369–11372
34 Tanaka H, Tabata H, Ota K, *et al.* Molecular-dynamics prediction of structural anomalies in ferroelectric and dielectric $BaTiO_3$-$SrTiO_3$-$CaTiO_3$ solid solutions. Phys Rev B, 1996, 53: 14112–14116
35 Davis L, Rubin LG. Some dielectric properties of barium-strontium titanate ceramics at 3000 megacycles. J Appl Phys, 1953, 24: 1194–1197
36 Kisaka S, Ikegami S, Sasaki H. Dielectric properties of mixed crystals of barium-strontium titanate. J Phys Soc Jpn, 1959, 14: 1680–1685

37 Nedelcu L, Toacsan MI, Banciu MG, *et al.* Dielectric properties of paraelectric $Ba_{1-x}Sr_xTiO_3$ ceramics. Ferroelectrics, 2009, 391: 33–41

38 Demirörs AF, Imhof A. $BaTiO_3$, $SrTiO_3$, $CaTiO_3$, and $Ba_xSr_{1-x}TiO_3$ particles: a general approach for monodisperse colloidal perovskites. Chem Mater, 2009, 21: 3002–3007

39 Yang J, Zhang J, Liang C, *et al.* Ultrathin $BaTiO_3$ nanowires with high aspect ratio: a simple one-step hydrothermal synthesis and their strong microwave absorption. ACS Appl Mater Interf, 2013, 5: 7146–7151

40 Sun H, Che R, You X, *et al.* Cross-stacking aligned carbon-nanotube films to tune microwave absorption frequencies and increase absorption intensities. Adv Mater, 2014, 26: 8120–8125

41 Pramanik NC, Anisha N, Abraham PA, *et al.* Preparation of $Ba_xSr_{1-x}TiO_3$ (x=0–1) nanoparticles by wet-chemical decomposition of Ti-complex and study their dielectric properties. J Alloy Comp, 2009, 476: 524–528

42 Chen X, Wang G, Duan Y, *et al.* Microwave absorption properties of barium titanate/epoxide resin composites. J Phys D-Appl Phys, 2007, 40: 1827–1830

43 Liu Y, Feng Y, Wu X, *et al.* Microwave absorption properties of La doped barium titanate in X-band. J Alloy Comp, 2009, 472: 441–445

44 Li J, Hietala S, Tian X. $BaTiO_3$ supercages: unusual oriented nanoparticle aggregation and continuous ordering transition in morphology. ACS Nano, 2015, 9: 496–502

45 Singh P, Babbar VK, Razdan A, *et al.* Complex permittivity, permeability, and X-band microwave absorption of CaCoTi ferrite composites. J Appl Phys, 2000, 87: 4362–4366

46 Che RC, Peng LM, Duan XF, *et al.* Microwave absorption enhancement and complex permittivity and permeability of Fe encapsulated within carbon nanotubes. Adv Mater, 2004, 16: 401–405

47 Meng XM, Zhang XJ, Lu C, *et al.* Enhanced absorbing properties of three-phase composites based on a thermoplastic-ceramic matrix ($BaTiO_3$ + PVDF) and carbon black nanoparticles. J Mater Chem A, 2014, 2: 18725–18730

48 Zhang XJ, Wang GS, Wei YZ, *et al.* Polymer-composite with high dielectric constant and enhanced absorption properties based on graphene-CuS nanocomposites and polyvinylidene fluoride. J Mater Chem A, 2013, 1: 12115–12122

Acknowledgments This work was supported by the National Natural Science Foundation of China (51471157, 21401183, 21431006 and 21521001), the National Basic Research Program of China (2014CB931800 and 2013CB931800), the Youth Innovation Promotion Association of CAS (2014298), Anhui Provincial Natural Science Foundation (1508085QB28), and the Fundamental Research Funds for the Central Universities (WK2060190026).

Author contributions Wu QS conducted the experiments, analyzed the results and wrote the paper; Yu SH and Liu JW supervised the project, conceived the experiments, analyzed the results and wrote the paper. Chen SF and Wang GS collected the data and analyzed the results. All authors contributed to the general discussion.

Conflict of interest The authors declare that they have no conflict of interest.

Supplementary information Experimental details are available in the online version of the paper.

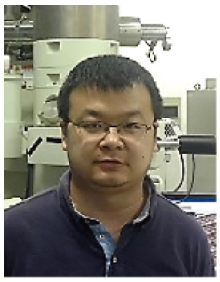

Qing-Song Wu received his PhD degree in materials physics and chemistry under the supervision of Prof. Shu-Hong Yu from the University of Science and Technology of China (USTC) in 2009. He is interested in the synthesis and application of perovskite nanomaterials.

Jian-Wei Liu received his BSc degree in chemical engineering and technology from Hefei University of Technology in 2007, and his PhD degree in nano-chemistry under the supervision of Prof. Shu-Hong Yu from the USTC. He is interested in the synthesis and self-assembly of one dimensional nanomaterials as well as nano-device fabrication based on well aligned nanowires.

Shu-Hong Yu received his BSc at Hefei University of Technology and his PhD degree (inorganic chemistry) from the USTC. He was a postdoctoral fellow with M. Yoshimura (Tokyo Institute of Technology) and a Humboldt Fellow with M. Antonietti and H. Cölfen (MPI of Colloids and Interfaces, Germany). In 2002, he was appointed the Cheung Kong Professor at USTC. Currently, he leads the Division of Nanomaterials & Chemistry at the Hefei National Laboratory for Physical Sciences at Microscale, USTC. His current research interests include bio-inspired synthesis and self-assembly of new nanostructured materials and nanocomposites, and their related properties. He serves as an editorial advisory board member of journals *Accounts of Chemical Research*, *Chemistry of Materials*, *Chemical Science*, *Materials Horizons*, *Nano Research*, *ChemNanoMat*, *CrystEngComm*, *Part. Part. Syst. Charact. and Current Nanoscience*. His recent awards include Chem. Soc. Rev. Emerging Investigator Award (2010) and Roy-Somiya Medal of the International Solvothermal and Hydrothermal Association (ISHA) (2010).

室温下无表面活性剂合成钛酸锶钡($Ba_xSr_{1-x}TiO_3$)纳米晶及其介电和微波吸收性能研究

吴庆松, 刘建伟*, 王广胜, 陈绍锋, 俞书宏*

摘要 因其优异的铁电、焦热电、介电、压电和电-光性能, 钙钛矿材料, 尤其是钛酸锶钡($Ba_xSr_{1-x}TiO_3$)受到了广泛且持续的关注. 本文报道一种简易温和的方法, 通过快速混合氯化钡、氯化锶水溶液和异丙醇钛的乙醇溶液, 无需表面活性剂和结构指引模板, 在室温下静置数小时即可制备钛酸锶钡($Ba_xSr_{1-x}TiO_3$)纳米晶, 其中, 钡/锶的摩尔比可以通过改变氯化钡和氯化锶的初始投料比精确调控. 我们对产物的介电性能和微波吸收性能进行了研究, 结果显示当$x = 0.7$时, 产物的介电性能和微波吸收性能达到最佳. 该合成方法条件温和、成本低廉且产率很高, 也为其他钙钛矿材料的制备提供了一条可能的新途径.